Materials Chemistry and Physics 172 (2016) 202–210

Contents lists available at ScienceDirect

Materials Chemistry and Physics

journal homepage: www.elsevier.com/locate/matchemphys

Synthesis of ceria (CeO_2 and CeO_{2-x}) nanoparticles via decarbonation and Ce(III) oxydation of synthetic bastnäsite ($CeCO_3F$)

German Montes-Hernandez [a, b, *], Rodica Chiriac [c], Nathaniel Findling [a, b], François Toche [c], François Renard [a, b, d]

[a] CNRS, ISTerre, F-38041 Grenoble, France
[b] Univ. Grenoble Alpes, ISTerre, F-38041 Grenoble, France
[c] Université de Lyon, Université Lyon 1, Laboratoire des Multimatériaux et Interfaces UMR CNRS 5615, 43 bd du 11 novembre 1918, 69622 Villeurbanne Cedex, France
[d] PGP, Department of Geosciences, University of Oslo, Box 1048 Blindern, 0316 Oslo, Norway

HIGHLIGHTS

- An original method to synthesize ceria nanoparticles (CeO_2 and CeO_{2-x}) from bastnäsite.
- New experimental conditions to produce ceria with oxygen vacancies CeO_{2-x}.
- (TGA/DSC) coupled with (μGC/MS) performed to investigate on the ceria formation.
- Specific hydrothermal conditions to which bastnäsite can be formed.

ARTICLE INFO

Article history:
Received 3 November 2015
Received in revised form
23 January 2016
Accepted 25 January 2016
Available online 2 February 2016

Keywords:
Inorganic compounds
Precipitation
Heat treatment
Crystallisation
Differential scanning calorimetry
Electron microscopy

ABSTRACT

Ceria (CeO_2) crystalline compound is widely used as a catalyst or catalyst support and many other applications. However, the studies are continuing with a view to improving existing methods and/or developing innovative routes to obtain well-controlled shapes and sizes of ceria nanoparticles. In the present study, we report an original method to synthesize ceria nanoparticles (CeO_2 and CeO_{2-x}) by using two independent stages: (1) the precipitation of bastnäsite-rich material under hydrothermal conditions (90 and 300 °C) and (2) the calcination of powdered basnäsite-rich material at different temperatures (500, 1000 and 1600 °C) and under different atmospheres (air, Ar, N_2 and secondary vacuum). In addition, simultaneous thermal analyses (TGA/DSC) coupled with gas chromatography (μGC/MS) were performed in order to investigate on the ceria formation during bastnäsite de-carbonation and its thermal behavior at high temperature (until 1600 °C) under three different gas atmospheres (air, Ar and N_2). Herein, ceria was in-situ formed independently on the gas investigated atmosphere. This means that sufficient oxygen was also available in the so-called inert atmospheres (Ar and N_2) to oxidize the Ce(III) contained in Ce-carbonates to Ce(IV) constituting ceria cubic structure. Moreover, μGC/MS measurements confirm that in-situ formed ceria CeO_2 at about 600 °C is then partially reduced to CeO_{2-x} at high temperature after 1000 °C because an increase in oxygen was clearly detected in expelled gas during heating process. This fundamental experimental study provides the hydrothermal conditions to which Ce fluorocarbonates could be formed in natural environments. In addition, new experimental conditions to produce ceria with oxygen vacancies CeO_{2-x} without reducing gas agent and at lower temperature are also provided in this study.

© 2016 Elsevier B.V. All rights reserved.

1. Introduction

Cerium being the most abundant metal among the rare earths, it is found in a number of minerals such as bastnäsite, monazite, gadolinite, fergusonite, samarskite, xenotime, yttrocerite, cerite,

* Corresponding author. CNRS, ISTerre, F-38041 Grenoble, France.
E-mail address: german.montes-hernandez@ujf-grenoble.fr (G. Montes-Hernandez).

http://dx.doi.org/10.1016/j.matchemphys.2016.01.066
0254-0584/© 2016 Elsevier B.V. All rights reserved.

allanite (or orthite), etc. Among these, bastnäsite fluorocarbonate ((Ce, La, Y)CO_3F) is the most important source of cerium and probably the most abundant in the nature [1–3]. Fluorocarbonates can have industrial applications related to their optical and magnetic properties, but, these rare minerals are systematically associated to other minerals and they systematically contain other structural rare or major elements that may restrict their utilization [3,4]. In this way, the synthesis of high-purity flurorocarbonates with controlled rare element composition, particle size and crystal morphology represent a significant challenge in materials science. Moreover, their precipitation under hydrothermal conditions could provide insights into the mobility of rare-earth elements during fluid–rock interactions in natural systems [5]. In this context, we report here specific hydrothermal conditions to which cerium fluorocarbonates such as bastnäsite ($CeCO_3F$) and Lukechangite ($Na_3Ce_2(CO_3)_4F$) could be formed in natural environments. We note that significant light rare earth elements (REE) reserves occur as fluorocarbonate minerals, mainly bastnäsite. However, despite the importance of these minerals, very little is known about the physicochemical conditions controlling their formation and experimental studies relevant to REE fluorocarbonate mineral stabilities are rare [6,7].

On the other hand, the cerium processed from bastnäsite and other natural cerium sources is typically used as ceria (CeO_2) nanoparticles or a wide variety of ceria-based nanomaterials (e.g. [8,9]). Ceria or cerium oxide exist also as natural mineral (called as cerianite) that has been identified as a secondary mineral at the many localities worldwide, including, weathered phonolites and nepheline syenites, hydrothermal veins, granite pegmatite, alluvial deposits, alkaline pegmatite, etc. [10], but, this accessory or minor mineral in host rocks is not directly exploited and used at our knowledge. Conversely, synthetic cerium oxide (CeO_2) having cubic structure is the most important oxide related to its extraordinary chemical properties (acid–base and oxidation-reduction behavior), thermal stability (melting point = 2400 °C) and oxygen mobility [9,11–13]. It has found its applications in catalysis, luminescent materials, fuel cell, free radical scavenger, gas sensor, cosmetic material, optical additives, polishing materials, water splitting, ceramic pigments, etc. [9,12,14–16]. However, the most important applications of ceria nanoparticles are as catalyst, catalyst promoters or catalyst supports. For example, control of toxic combustion gas emissions (e.g. in automobile mufflers) via oxidation of CO and reduction of NO_x [9 and references therein]. This is due to high oxygen mobility allowing reversible reduction-oxidation cyclic reactions without disruption of the cubic lattice-structure [17]. Due to numerous applications of ceria, several methods of synthesis have been proposed in the last two decades such as sol–gel process, aqueous precipitation, electrochemical synthesis, hydrothermal and solvothermal synthesis routes, reverse micellar synthesis, microemulsion method, flame spray pyrolysis, sonochemical method, microwave-assisted method, etc. (e.g. [9,11,12,18]). Several of above methods require a second independent step by thermal treatment or so-called calcination ($T \geq 500$ °C) in order to obtain high-purity CeO_2 material. Studies are continuing with a view to improving existing methods and/or developing innovative routes to obtain well-controlled shapes and sizes of ceria nanoparticles.

The purpose of the present study was two-fold. Firstly, synthesize high-purity bastnäsite ($CeCO_3F$) using hydrothermal conditions. As above mentioned, bastnäsite is the most important source of cerium, but, very little is known about the physicochemical conditions controlling its formation in natural settings [6,7]. Herein, we provide specific hydrothermal conditions to which bastnäsite can be formed, but, it has coexisted with Petersenite $Na_4Ce_2(CO_3)_5$ and/or Lukechangite $Na_3Ce_2(CO_3)_4F$ depending on the temperature, both in minor proportion. Secondly, synthesize ceria CeO_2 nanoparticles by direct calcination of synthetic bastnäsite. For this purpose, recovered powdered Ce-carbonate material was calcined under air or secondary vacuum ($\approx 5 \times 10^{-6}$ mbar) at 500 or 1000 °C in a quartz tubular reactor. As expected, high-purity ceria CeO_2 nanoparticles (S_{BET} = 30 m^2/g) were obtained in air atmosphere, while CeO_{2-x} partially reduced ceria nanoparticles (S_{BET} = 10 m^2/g) were obtained under secondary vacuum. In complement to this basic investigation, simultaneous thermal analysis (TGA/DSC) coupled with gas chromatography (μGC/MS) were performed in order to investigate on the ceria formation during bastnäsite de-carbonation under non-isothermal conditions and its thermal behavior at high temperature (until 1600 °C) under three different gas atmospheres (air, Ar and N_2).

2. Materials and methods

2.1. Precipitation of bastnäsite fluorocarbonate $CeCO_3F$

250 ml of high-purity water with electrical resistivity of 18.2 MΩ cm, 10 g of NaOH, 12.5 g of $CeCl_3.7H_2O$ and 2.1 g of NaF were placed in a reactor (hastelloy C22 autoclave with internal volume of 0.6 L). This reactive suspension was immediately stirred during the reaction by means of a constant mechanical stirring system (400 rpm). The temperature of the suspension increased instantaneously to 26 °C due to the exothermic dissolution of NaOH in the system. At this reference temperature, CO_2 was immediately injected in the system at a pressure of 40 bar. The carbonation reaction started instantaneously as attested by the continuous consumption of CO_2, monitored by a pressure drop in the system, and an increase in temperature during the exothermic carbonation reaction. After about 5 h of carbonation reaction, a heat-aging step was performed from room temperature to 300 °C for a further 24 h. Herein, the total pressure was stabilized to 93 bar at 300 °C. The same synthesis procedure was also performed at 90 °C.

At the end of the experiment, the autoclave was removed from the heating system and cooled using continuous flow air. The residual CO_2 was degassed from the reactor after air-cooling period, i.e. when $T \leq 60$ °C. After water cooling at 60 °C the autoclave was disassembled, and the solid product was carefully recovered and separated by centrifugation (30 min at 12,000 rpm), decanting the supernatant solutions. The solid product was washed twice by redispersion/centrifugation processes in order to remove the soluble sodium carbonates formed during the synthesis. Finally, the solid product was dried directly in the centrifugation flasks at 80 °C for 48 h. The dry solid product was manually recovered and stored in plastic flasks for subsequent characterization (FESEM, XRD, TGA/DSC and N_2 sorption isotherms).

2.2. Synthesis of ceria CeO_2 nanoparticles by calcination

1 or 2 g of dry synthetic bastnäsite ($CeCO_3F$)-rich material (purity ≈ 70%) mixed with two other Ce carbonates (Petersenite (20%): $Na_4Ce_2(CO_3)_5$ and Lukechangite (10%): $Na_3Ce_2(CO_3)_4F$) obtained from above hydrothermal method (sub-Section 2.1) were thermally treated under air atmosphere or secondary vacuum ($\approx 5 \times 10^{-6}$ mbar) by using a quartz tubular reactor. Herein, two temperatures (500 and 1000 °C) were typically investigated. The same heating rate (30 °C/min) was used in all experiments. The duration of thermal treatment was arbitrary defined at five hours, but, for some experiments performed at 500 °C, the duration was prolonged to 4 days in order to investigate on the kinetics effect. At the end of experiment, the samples were cooled under their original atmosphere, i.e. in contact with atmospheric air or under vacuum. The dry solid product was manually recovered and stored

in plastic flasks for subsequent characterization (FESEM, XRD, TGA/DSC and N_2 sorption isotherms).

2.3. Characterization of the solid products

X-Ray Powder Diffraction (XRD) analyses were performed using a Siemens D5000 diffractometer in Bragg-Brentano geometry; equipped with a theta–theta goniometer with a rotating sample holder. The XRD patterns were collected using Cu $k\alpha_1$ ($\lambda_{k\alpha1} = 1.5406$ Å) and $k\alpha_2$ ($\lambda_{k\alpha2} = 1.5444$ Å) radiation in the range $2\theta = 10–70°$ with a step size of 0.04° and a counting time of 6 s per step. Ceria (CeO_2), ceria with oxygen vacancies (CeO_{2-x}), Ce_7O_{12} and villiaumite (NaF) crystal structures were systematically refined by Rietveld method on XRD patterns using the BGMN software and its associated database [19]. In complement to this phase composition, "x" parameter in CeO_{2-x} phase (corresponding to oxygen vacancies) was roughly determined by linear interpolation between CeO_2 and CeOF cubic structures.

FESEM observations: Selected samples containing ceria or bastnäsite were dispersed by ultrasonic treatment in absolute ethanol for five to ten minutes. One or two droplets of the suspension were then deposited directly on an aluminum support for SEM observations, and coated with platinum. The morphology of crystal faces was observed by using a Zeiss Ultra 55 field emission gun scanning electron microscope (FESEM) with a maximum spatial resolution of approximately 1 nm at 15 kV.

Thermogravimetric analyses: TGA for all bastnäsite or ceria samples were performed with a Mettler Toledo TGA/DSC 2 instrument under the following conditions: sample mass of about 10 mg, 150 μL platinum crucibles with a pierced lid, heating rate of 5, 10 or 20 °C min^{-1}, and inert N_2 and Ar, and air atmosphere of 50 mL min^{-1}. Sample mass loss and associated thermal effects were obtained by TGA/DSC. In order to identify the different mass loss steps, the TGA first derivative (rate of mass loss) was used. The calibration of TGA apparatus in the conditions of our measurements was checked in terms of mass loss and temperature. Calcium oxalate was used for the sample mass calibration check. The melting points of three compounds (indium, aluminum and copper) obtained from the DSC signals were used for the sample temperature calibration.

N_2 sorption isotherms: N_2 sorption isotherms for two ceria samples were obtained by using the BelSorp Mini II (Bel Japan) analyzer. The samples were properly degased before measurements. The specific surface area of powdered samples was estimated by applying the Brunauer-Emmet-Teller (BET) equation in the $0.05 \leq P/P_0 \leq 0.35$ interval of relative pressure and based on a value of 16.2 $Å^2$ for the cross-sectional area of molecular N_2. A non-linear regression by the least-squares method was performed to fit the interval data (n_{ads} *vs.* P/P_0) in the experimental isotherms.

2.4. Thermal behavior by TGA/DSC coupled with μGC-MS

The evolved gases (CO_2, H_2O) were analyzed with a portable micro-gas chromatograph μGC (SRA Instruments) coupled to a mass spectrometer detector Agilent 5973 Network. The μGC is equipped with 3 modules, each one composed of a column and a thermal conductivity detector (TCD). For our measurements, the CO2 and H2O gases have been followed on the Poraplot U capillary column and the O_2 gas was followed on the molecular sieve column. Helium was used as carrier gas. The molecular sieve and Poraplot U column temperatures were fixed at 70 °C and 90 °C respectively. The inject time was of 200 msec for both columns, and a backflush time of 6 s was used for the molecular sieve column. The head column pressure was fixed at 28 psi for the molecular sieve column and 30 psi for Poraplot U column. CO_2 was separated within 20 s, while H_2O within 80 s. Samplings of evolved gases during TGA analysis have been done every 2 or 4–5 min depending on mass loss steps.

3. Results and discussion

3.1. Bastnäsite precipitation: reaction mechanism

Bastnäsite fluorocarbonate is the main natural source of cerium in the world; however, little is known on its formation conditions, reaction mechanisms and crystal growth process. In the present experimental study, we report that bastnäsite mineral can be successfully formed between 90 and 300 °C in high-carbonate alkaline media as revealed by x-ray diffraction on obtained solid products (Fig. 1: more details are provide below). Assuming that CO_2 absorption in the highly alkaline solution of NaOH (1 M) is faster and greater than in high-purity water via the following sequential exothermic reactions:

$$2NaOH + CO_{2(aq)} \rightarrow Na_2CO_3 + H_2O \quad (1)$$

$$Na_2CO_3 + H_2O + CO_{2(aq)} \rightarrow 2Na^+ + 2HCO_3^- \quad (2)$$

the precipitation of bastnäsite fluorocarbonate can be then written as follows:

$$Ce^{3+} + F^- + HCO_3^- \rightarrow Ce(CO_3)F + H^+ \quad (3)$$

Fluor and Ce(III) ions in the reaction 3 from respective instantaneous dissolution of NaF and $CeCl_3$ in the system, probably, cerium ions are firstly hydrolyzed forming a cerium hydroxide precursor, but, this expected step was not measured/observed in our batch reaction experiments. In fact, in our investigated conditions, bastnäsite has co-existed with lukechangite ($Na_3Ce_2(CO_3)_4F$: 13 wt%) and petersenite ($Na_4Ce_2(CO_3)_5$: 17 wt%) at 300 °C and only with petersenite (8 wt%) at 90 °C as determined by Rietveld refinement of XRD patterns (see also Fig. 1). Temperature has also controlled the textural properties for bastnäsite; for example, oriented nanoparticles (<50 nm) forming spherical aggregates (3D objects forming mesocrystals (e.g. [20–22])) were obtained at 90 °C

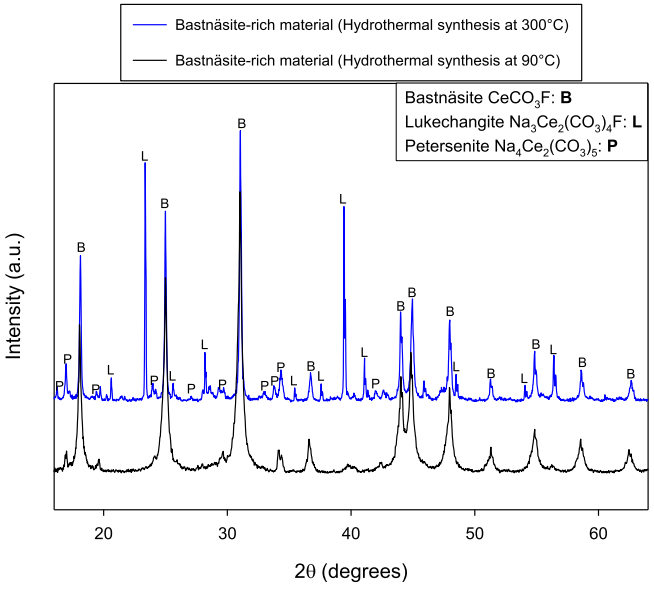

Fig. 1. XRD experimental patterns for bastnäsite-rich material precipitated at 90 and 300 °C.

while nanoparticles (>50 nm) forming irregular aggregates were obtained at 300 °C (see FESEM images in Fig. 2). In summary, more complex mineral composition and diversified crystal morphologies, particle sizes and aggregation states were obtained at 300 °C. For this reason, the following sub-sections in the results and discussion will be mainly focused on the bastnäsite-rich material precipitated at 300 °C; but we conclude here that the bastnäsite mineral can be formed in a wide temperature range (at least from 90 to 300 °C) in alkaline environments.

3.2. Bastnäsite-to-ceria solid state transformation and reaction mechanisms

Bastnäsite ($Ce(CO_3)F$) de-carbonation by thermal treatment in air atmosphere implies simultaneously the Ce(III) oxidation to Ce(IV), leading to the formation of ceria (CeO_2) and expelling CO_2 and F_2 gases. Unfortunately, scanty studies investigating on this double-reaction have been reported in the literature. In this way, a recent study has reported that the natural bastnäsite de-carbonation follows a single reaction ($Ce(CO_3)F \rightarrow CeOF + CO_2$). This was incorrectly interpreted because the reported XRD patterns after thermal treatment, reveals only ceria (CeO_2) as product (see Fig. 9 in reference [7]). In the present study, our results have confirmed that bastnäsite ($Ce(CO_3)F$) de-carbonation by thermal treatment in air, N_2 or Ar atmospheres or under secondary vacuum ($\approx 5 \times 10^{-6}$ mbar) implies simultaneously the Ce(III) oxidation to Ce(IV), leading to the formation of ceria (CeO_2) (see Figs. 3 and 4). For example, the bastnäsite-rich material thermally treated in a quartz tubular reactor at 500 °C for 4 h in air atmosphere, leads to crystalline ceria and NaF products as revealed by x-ray diffraction (Fig. 3) and confirmed by simultaneous thermal analysis (TGA/DSC) up to 1000 °C (Fig. 4). Even if the TGA curve shows a single mass loss step probably corresponding to the CO_2 expelling one can see on DSC signal an endothermic phenomenon composed of 3 overlapped peaks. The formation mechanism of ceria and NaF is in fact a multistep de-carbonation reaction as the synthesized bastnasite is mixed with 2 other carbonates. In contrast, when secondary

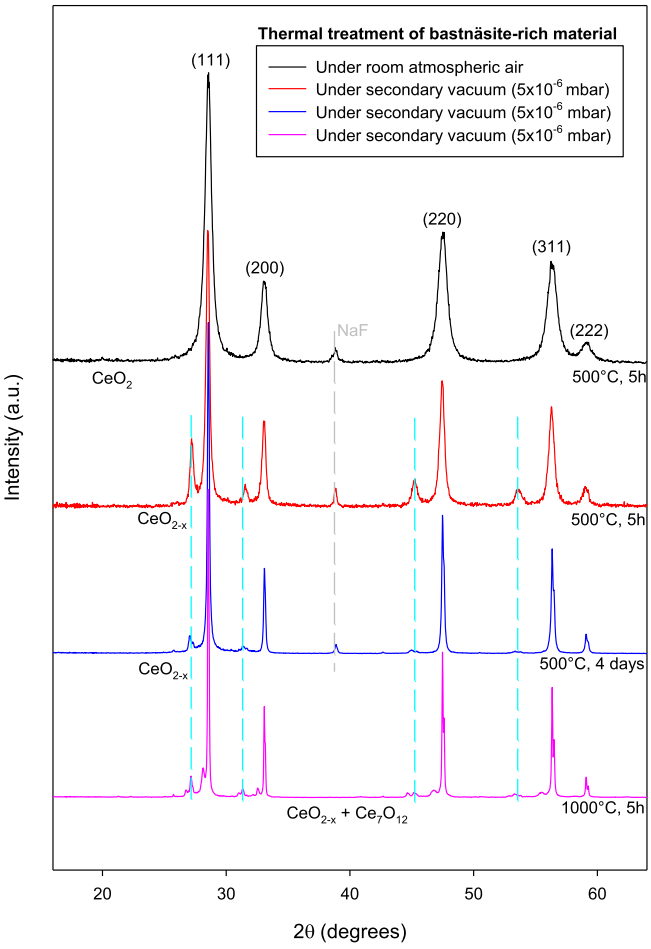

Fig. 3. XRD experimental patterns for powdered ceria obtained from calcination of bastnäsite-rich material in air atmosphere and secondary vacuum.

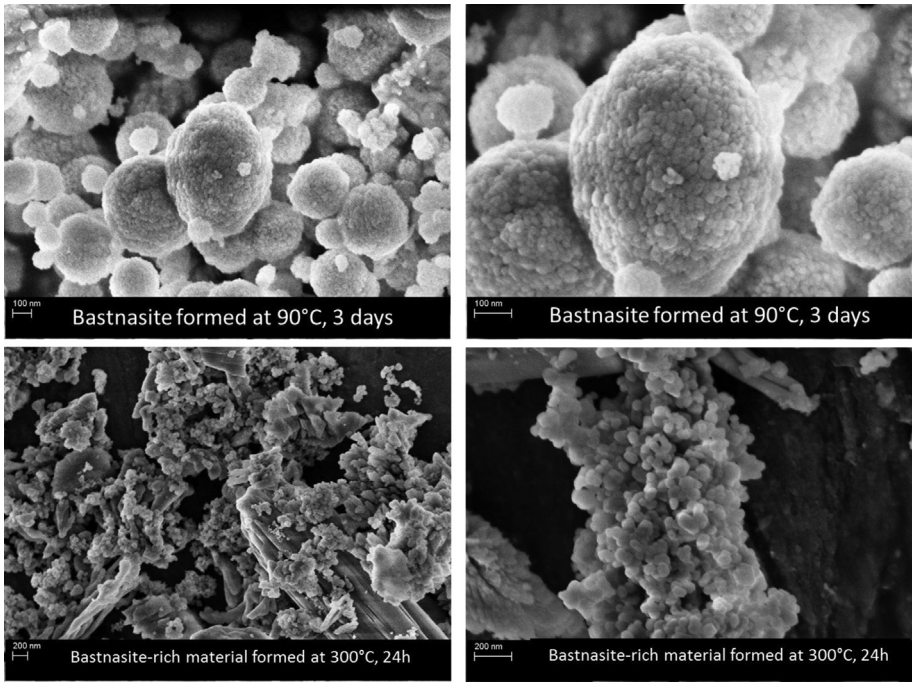

Fig. 2. FESEM images at two different magnifications for bastnäsite-rich material precipitated at 90 and 300 °C.

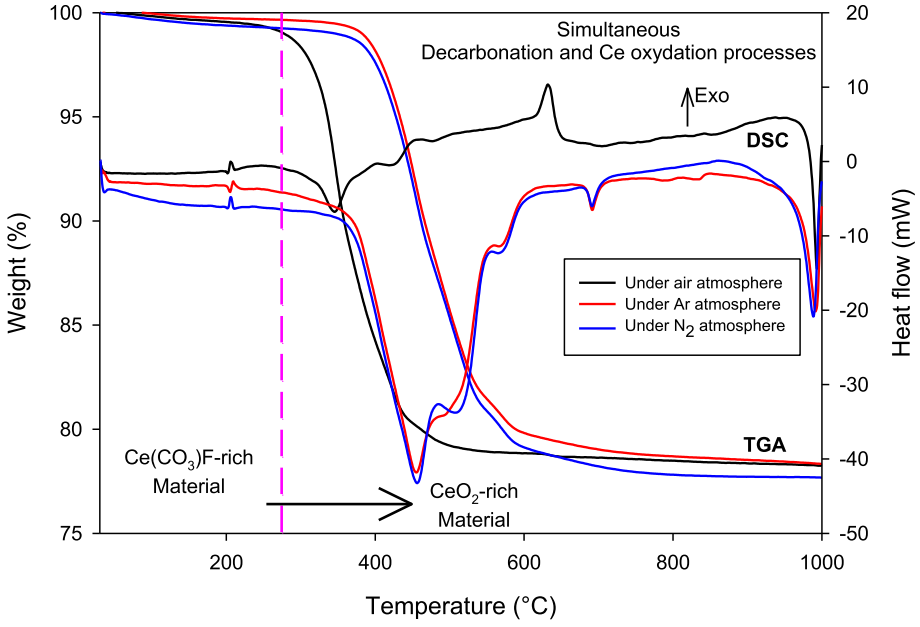

Fig. 4. Simultaneous TGA/DSC measurements (heating rate = 10 °C/min) for non-isothermal (up to 1000 °C) decomposition of bastnäsite-rich material under different gas atmospheres (air, N_2 and Ar).

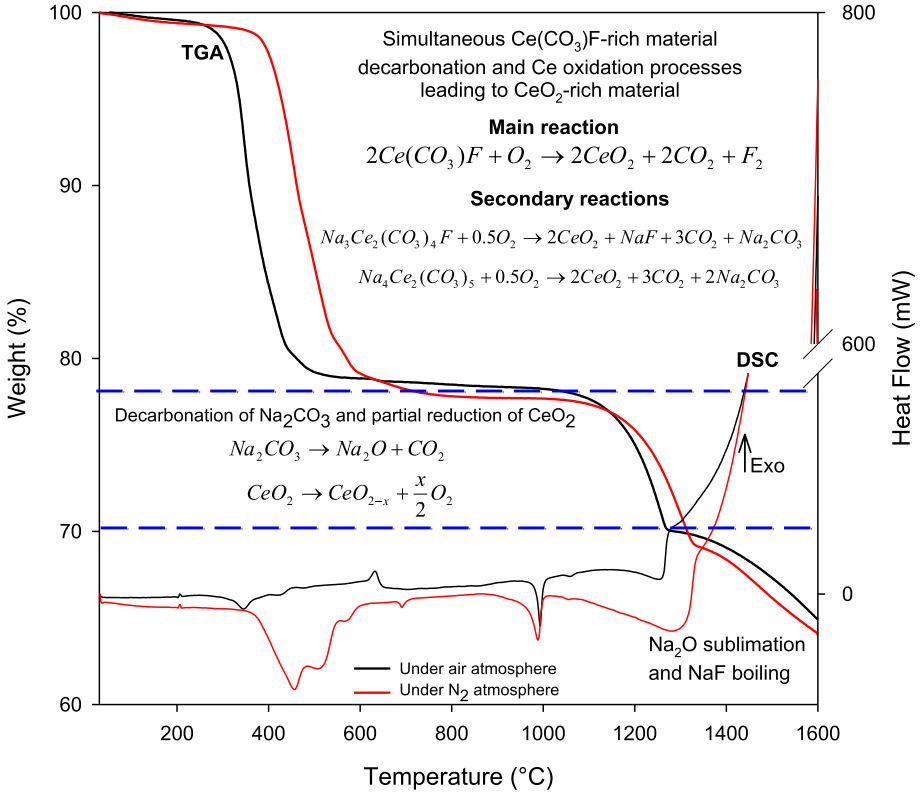

Fig. 5. Simultaneous TGA/DSC measurements (heating rate = 10 °C/min) for non-isothermal (up to 1600 °C) decomposition of bastnäsite-rich material under two different gas atmospheres (air and N_2) including the implied multi-reactions. We note that the proposed reactions were supported by XRD and μ-GC-MS complementary measurements.

vacuum was used, ceria with oxygen vacancies (CeO_{2-x}) was systematically obtained at 500 and 1000 °C (see Fig. 3). Moreover, Ce_7O_{12} phase with hexagonal crystal structure was also identified when bastnäsite-rich material was treated at 1000 °C under secondary vacuum and the NaF salt was not more detected on the XRD pattern (Fig. 3: run 1000 °C, 5 h). This means that more reducing conditions were created at higher temperature as typically assumed in the literature (e.g. [14,16,23]). These simple experiments have demonstrated that secondary vacuum is not enough to stabilize Ce(III) as CeOF compound from bastnäsite de-carbonation,

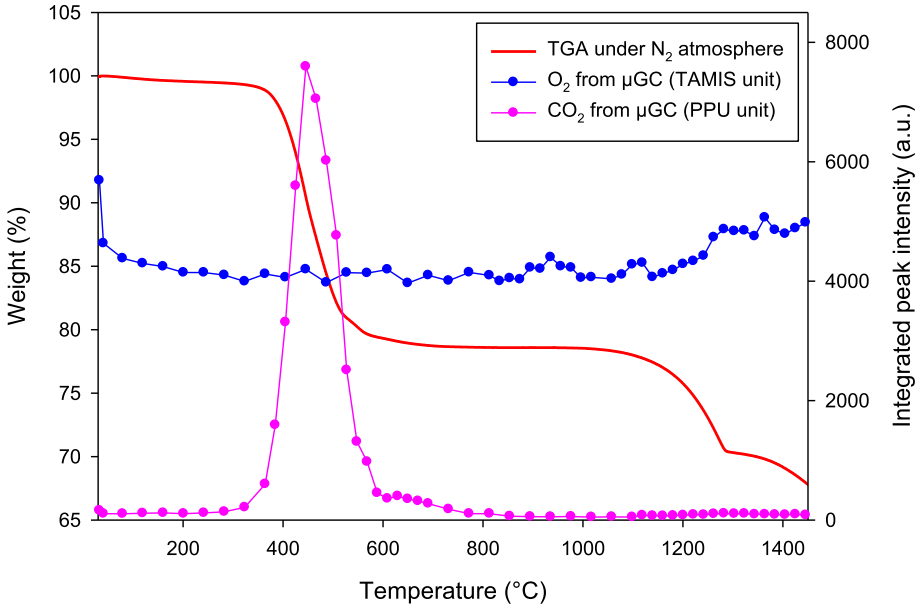

Fig. 6. Coupling TGA/DSC with µGC measurements for non-isothermal (up to 1450 °C) decomposition of bastnäsite-rich material under N_2 atmosphere. These results have supported the reaction mechanisms described in the text and in Fig. 5.

contrary to the de-carbonation reaction mechanism reported by Gysi and Williams-Jones [7]. However, the available oxygen in the system can be rapidly sequestered by cerium oxidation from Ce(III) to Ce(IV) that creates then a powerful reducing environment in the vacuum tubular cell. To confirm this idea, synthetic high-purity goethite was treated at 500 °C under secondary vacuum in presence and in absence of bastnasite-rich material (without solid−solid contact). These simple experiments confirm that the goethite (FeOOH) treated in absence of bastnäsite leads the hematite (Fe_2O_3) formation co-existing with a minor proportion of magnetite ($FeO*Fe_2O_3$ or Fe_3O_4). Conversely, goethite is highly transformed to magnetite mineral when the thermal treatment under vacuum at 500 °C is performed in presence of bastnasite (see Fig. SI-1). These original redox reactions attest that the Ce(III) contained initially in cerium carbonates (bastnäsite-rich material) was oxidized to Ce(IV) to form ceria (CeO_{2-x}) while a part of Fe(III) initially contained in goethite (FeOOH) was reduced to form preferentially magnetite (Fe_3O_4) in the system. These new results open new possibilities to synthesize magnetite or magnetite composites (materials with significant catalytic properties (e.g. [24])) by simple thermal treatment of goethite in presence of bastnäsite without use of gas reducing agents. These new results will be reported in a specific research study.

3.2.1. Reaction mechanism

The bastnäsite-rich material that precipitated at 300 °C is composed by three cerium carbonates, basnäsite ($Ce(CO_3)F$), lukechangite ($Na_3Ce_2(CO_3)_4F$) and petersenite ($Na_4Ce_2(CO_3)_5$). XRD and TGA/DSC up to 1000 °C have only revealed the formation of ceria (CeO_2) and NaF. Unfortunately, these two reaction products cannot completely explain the reaction mechanism during calcination process. In order to resolve this inconsistency, simultaneous thermal analysis (TGA/DSC) up to 1600 °C coupled to µGC/MS were performed. TGA curves have revealed two successive significant mass losses at high temperature (>1000 °C): the first mass loss comprised between 1100 and 1300 °C is related to the endothermic decomposition of in-situ formed Na_2CO_3 and partial (endothermic) reduction of CeO_2, and the second mass loss comprised between 1300 and 1600 °C is attributed to the sublimation of Na_2O and boiling of NaF. Sublimation and boiling are endothermic phenomena and not exothermic as revealed by the strong increase of DSC signal at temperatures higher than 1300 °C. This could be explained by the presence of another phenomenon, which is highly exothermal, taking place in the same time with the 2 endothermal phenomena and thus the endothermal peak is overlapped by the exothermal one. The fact that the DSC signal become highly exothermic after 1300 °C could be explained by the condensation of emitted vapors on TGA sensor. This is supported by the color change from white to gray observed on TGA sensor at the end of TGA analysis.

The sublimation of Na_2O takes place before the boiling of NaF if we take into consideration the literature values for these two compounds: 1275 °C for Na_2O and 1695 °C for NaF. In our case the thermal phenomena take place earlier, especially in the case of NaF, and this could be explained by several factors giving a synergetic effect, such as: (*i*) the fact that the two compounds are mixed and not present separately as pure compounds, (*ii*) the platinum crucible acts as catalyzer at very high temperatures and (*iii*) the submicrometric sizes of the particles. Also, the thermal phenomena take place at lower temperatures when air is used at reactive gas and this could be seen on Fig. 5 when comparing the DSC signals under air, N_2 and Ar. The endothermal phenomena taking place in a temperature range with no mass loss (*i.e.* between 900 and 1100 °C) could correspond to the melting of Na_2CO_3, NaF and Na_2O (the melting temperatures of these 3 compounds, as given in the literature, are 854, 993 and 1132 °C respectively).

The complete reaction mechanism implying the three initial Ce carbonates in bastnäsite-rich material synthesized at 300 °C can be written as follows:

1) De-carbonation and cerium oxidation processes from 400 to 1000 °C

$$2Ce(CO_3)F + O_2 \rightarrow 2CeO_2 + 2CO_2 + F_2 \ldots (\text{Main reaction}) \quad (4)$$

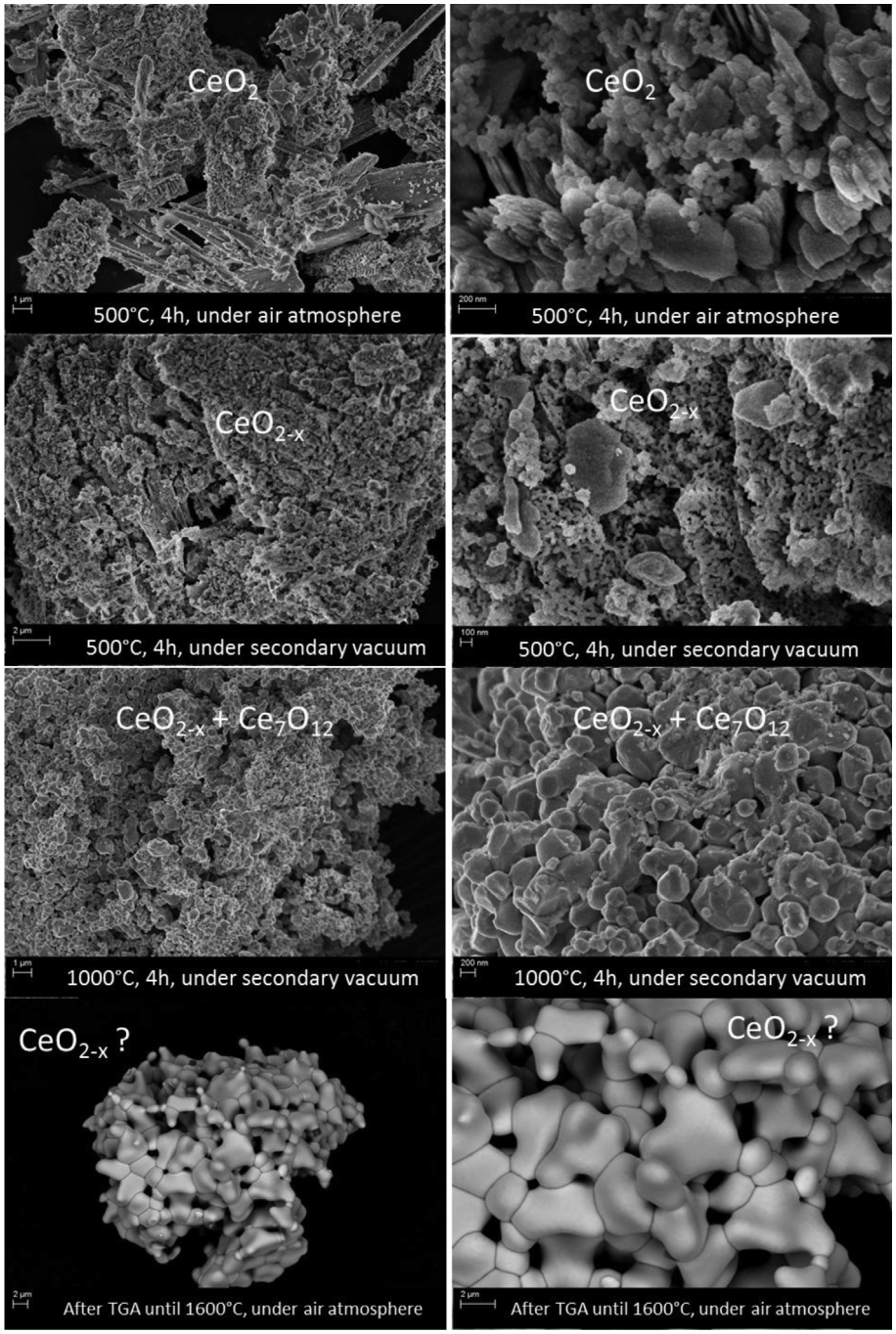

Fig. 7. FESEM images at two different magnifications for ceria produced from bastnäsite-rich material calcination at different atmosphere (air and secondary vacuum) and temperature (500, 1000 and 1600 °C).

$$Na_3Ce_2(CO_3)_4F + 0.5O_2 \rightarrow 2CeO_2 + NaF + 3CO_2 + Na_2CO_3 \ldots (\text{Secondary reaction}) \quad (5)$$

$$Na_4Ce_2(CO_3)_5 + 0.5O_2 \rightarrow 2CeO_2 + 3CO_2 + 2Na_2CO_3 \ldots (\text{Secondary reaction}) \quad (6)$$

2) De-carbonation of in-situ formed Na_2CO_3 and partial reduction of CeO_2 from 1000 to 1300 °C

$$Na_2CO_3 \rightarrow Na_2O + CO_2 \quad (7)$$

$$CeO_2 \rightarrow CeO_{2-x} + \frac{x}{2}O_2 \quad (8)$$

3) Sublimation of Na_2O and boiling of NaF from 1300 to 1600 °C

This complex reaction mechanism was directly summarized on the TGA/DSC curves (Fig. 5). Moreover gas chromatography (μGC) measurements of expelled gases up to 1450 °C support strongly this

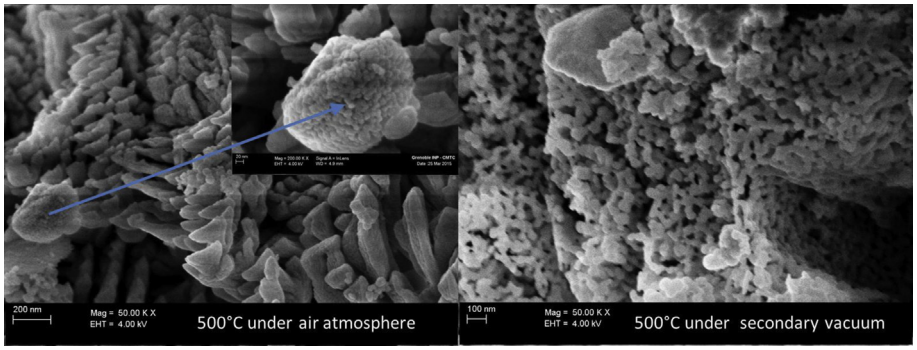

Fig. 8. FESEM images showing ceria nanoparticles produced from bastnäsite-rich material calcination at 500 °C under air atmosphere and secondary vacuum.

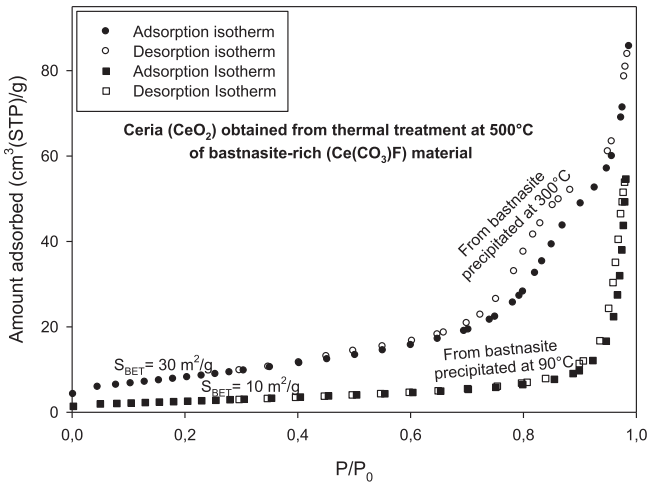

Fig. 9. N_2 adsorption–desorption isotherms of ceria produced by simple calcination of bastnäsite-rich material in air atmosphere.

suggested reaction mechanism (Fig. 6). In Fig. 6, the CO2 and O2 evolutions with the increasing TGA temperature are superposed with the TGA curve. Each point on the gas evolution curve represents the area of the gas peak at a fixed temperature during TGA analysis. In fact, μGC measurements confirm a major production of CO_2 between 350 and 600 °C related to de-carbonation processes (see reactions 3 to 5 above). In addition, the slight oxygen and carbon dioxide production at high temperatures support the reactions 7 and 8.

3.3. Some textural properties of ceria

The industrial applications of solid compounds are frequently related to their textural properties such as average particle size, particle size distribution, crystallinity and morphology of crystals, specific surface area and aggregation state (e.g. [25–27]). The present study reports that the ceria obtained by calcination of bastnäsite-rich material has irregular particular size. In fact, nanoparticles forming irregular aggregates co-exist with micrometric dense conglomerates (in minor proportion) as observed on FESEM images (runs: 500 °C, 4 h, in air and 500 °C, 4 h, under vacuum in Fig. 7). Herein, nanoparticles were clearly observed on FESEM images at high magnification for ceria obtained at 500 °C (see Fig. 8). In addition, N_2 sorption/desorption isotherms have revealed that the ceria powdered material is slightly porous (slight desorption hysteresis) with a modest specific surface area (30 m^2/g) (Fig. 9). Surprisingly, the specific surface area of ceria is lower when calcination step is performed under secondary vacuum (9 m^2/g). Another surprising result, it was that the calcination of bastnäsite precipitated at 90 °C, initially porous material with moderate specific surface area (40 m^2/g), has led to non-porous ceria material with lower specific surface area (10 m^2/g) (Fig. 9). For our basic study, the bastnäsite-rich material precipitated at 300 °C allows the obtaining better textural properties of ceria by simple calcination under air atmosphere. However, the high-purity bastnäsite (or cerium fluorocarbonate: $CeCO_3F$) precipitated at 90 °C could find specific applications because it is a mesoporous material with moderate specific surface area (40 m^2/g) and the constituting nanoparticles form regular spherical aggregates (similar to the so-called mesocrystals [26]) that allow the most easy manipulation with respect to isolated nanoparticles.

As expected, the particle size of synthesized ceria has increased with calcination temperature. Herein, sub-micrometric rounded particles were obtained at 1000 °C and micrometric particles at 1600 °C (See last FESEM images in Fig. 7).

4. Conclusion

The present study has reported an original method to synthesize ceria nanoparticles (CeO_2 and CeO_{2-x}) by using two independent stages: firstly, the precipitation of bastnäsite-rich material under hydrothermal conditions (90 and 300 °C) and secondly, the calcination of powdered basnäsite-rich material at different temperatures (500, 1000 and 1600 °C) and under different atmospheres (air, Ar, N_2 and secondary vacuum). In this study, fundamental investigation was carried out; for example, we provide hydrothermal conditions to which Ce fluorocarbonates can be formed in natural environments. In addition, a significant effort was devoted to determine clearly the implied multi-reactions during calcination process of bastnäsite-rich material by coupling simultaneous thermal analysis (TGA/DSC) with gas chromatography (μGC/MS). These results were also supported by x-ray diffraction (XRD) analyses. In this way, new experimental conditions to produce high-purity ceria (with or without oxygen vacancies CeO_{2-x}) are provided in this study.

Acknowledgments

The authors are grateful to the French National Center for Scientific Research (CNRS), the Universite Grenoble Alpes, the Labex OSUG@2020 (Investissement d'avenir-ANR10-LABX56), and the ANR French research agency (ANR SPRING project) for providing funding support.

Appendix A. Supplementary data

Supplementary data related to this article can be found at http://dx.doi.org/10.1016/j.matchemphys.2016.01.066.

References

[1] M. Mohapatra, V. Natarajan, R. Rajeswari, A.R. Dhobale, S.V. Gogbole, J. Lumin. 145 (2014) 105–109.
[2] L. Wang, C. Wang, Y. Yu, X. Huang, J. Hazard. Mater. 209–210 (2012) 77–83.
[3] J.D. Grice, G.Y. Chao, Amer. Min. 82 (1997) 1255–1260.
[4] G. Mongelli, Chem. Geol. 140 (1997) 69–79.
[5] E. Roberti, G.E.R. Enrich, C.B. Gomes, Comin-Chiaramunti Can. Min. 46 (2008) 901–914.
[6] A.E. Williams-Jones, S.A. Wood, Geochem. Cosmochem. Acta 56 (1992) 725–738.
[7] A. Gysi, A.E. Williams-Jones, Chem. Geol. 392 (2015) 87–101.
[8] Q. Yuan, H.H. Duan, L.L. Li, L.D. Sun, Y.W. Zhang, C.H. Yan, J. Colloid Interface Sci. 335 (2009) 151–167.
[9] A. Bumajdad, J. Eastoe, A. Mathew, Adv. Colloid Interface Sci. 147–148 (2009) 56–66.
[10] A.N. Zaitsev, E.Y. Avdontseva, S.N. Britvin, A. Demény, Z. Homonnay, T. Jeffries, J. Keller, V.G. Krivovichev, G. Markl, N.V. Platonova, O.I. Siidra, J. Spratt, IMA 2011-035, Ferrikaersutite 75 (2011) 2549–2561.
[11] E. Leino, P. Maki-Arvela, V. Eta, N. Kumar, F. Demoisson, A. Samikannu, A.R. Leino, A. Shchukarev, D.Y. Murzin, J.P. Mikkola, Catal. Today 210 (2013) 47–54.
[12] S. Soren, M. Bessoi, P. Parhi, Ceram. Int. 41 (2015) 8114–8118.
[13] E. Leino, N. Kumar, P. Maki-Arvela, A. Aho, K. Kordas, A.R. Leino, A. Shchukarev, D.Y. Murzin, J.P. Mikkola, Mater. Chem. Phys. 143 (2013) 65–75.
[14] N. Gokon, S. Sagawa, T. Kodoma, Int. J. Hydrogen Energy 38 (2013) 14402–14414.
[15] T. Yousefi, A.N. Golikand, M.H. Mashhadizadeh, Mater. Sci. Semicond. Process 16 (2013) 1943–1948.
[16] S. Abanades, G. Flamant, Sol. Energy 80 (2006) 1611–1623.
[17] A. Trovarelli, Catal. by ceria Relat. Mater. (2002), 528pp.
[18] S. Thakur, P. Patil, Sens. Actuat. B-Chem. 194 (2014) 260–268.
[19] T. Taut, R. Kleeberg, J. Bergmann, Mater. Sci. Bull. Czech Slovak Crystallogr. Assoc. 5 (1988) 55–64.
[20] R.Q. Song, H. Cölfen, Adv. Mater 22 (2010) 1301–1330.
[21] H. Cölfen, M. Antonietti, Angew. Chem. Int. Ed. 44 (2005) 5576–5591.
[22] L. Zhou, P. O'Brien, J. Phys. Chem. Lett. 3 (2012) 620–628.
[23] P. Charvin, S. Abanades, E. Bech, F. Lemont, G. Flamant, Solid State Ionics 180 (2009) 1003–1010.
[24] Z. Wen, Y. Zhang, C. Dai, Z. Sun, J. Hazard. Mater. 287 (2015) 225–233.
[25] G. Montes-Hernandez, A. Fernandez-Martinez, L. Charlet, D. Tisserand, F. Renard, J. Cryst. Growth 310 (2008) 2946–2953.
[26] G. Montes-Hernandzez, R. Renard, N. Findling, A.L. Auzende, CrystEngComm 17 (2015) 5725–5733.
[27] G. Montes-Hernandez, D. Daval, R. Chiriac, F. Renard, Cryst. Growth Des. 10 (2010) 4823–4830.